High Power Laser Science and Engineering, (2016), Vol. 4, e5, 12 pages.

doi:10.1017/hpl.2016.1

Measuring vacuum polarization with high-power lasers

B. King and T. Heinzl

Centre for Mathematical Sciences, Plymouth University, Plymouth PL4 8AA, United Kingdom

(Received 21 November 2015; accepted 12 January 2016)

Abstract

When exposed to intense electromagnetic fields, the quantum vacuum is expected to exhibit properties of a polarizable medium akin to a weakly nonlinear dielectric material. Various schemes have been proposed to measure such vacuum polarization effects using a combination of high- power lasers. Motivated by several planned experiments, we provide an overview of experimental signatures that have been suggested to confirm this prediction of quantum electrodynamics of real photon–photon scattering.

Keywords: Heisenberg–Euler; photon–photon scattering; vacuum birefringence; vacuum polarization

1. Motivation

The increasing availability of multi-hundred TW and PW lasers[1] brings the confirmation of long-predicted phenomena of strong-field quantum electrodynamics (QED)[2, 3] closer. A multitude of effects on the polarization, wavevector and frequency of photons that probe the polarization of the charged virtual pairs of the vacuum have been theoretically investigated. All of these effects can be understood in terms of the single process of 'photon–photon scattering'. The current best experimental limit on the predicted cross-section for photon–photon scattering using just high-power laser pulses lies eighteen orders of magnitude above QED[4], but recent laser-cavity experiments such as BMV[5] and PVLAS[6] have reduced this to six and three orders of magnitude, respectively (or three orders of magnitude and a factor 50, respectively, at the level of the refractive index). Moreover, coinciding with the completion of the XFEL laser at DESY, an experiment at the HIBEF facility[7] plans to measure one manifestation of photon–photon scattering, namely the birefringence of the vacuum, using the XFEL beam and a 1 PW optical laser. This has generated much interest in vacuum polarization effects.

The aims of this work are two-fold. First, the main analytical approaches used to study photon–photon scattering will be shown to be essentially equivalent for predictions of planned laser experiments. Second, an overview of the predicted signatures of real photon–photon scattering in various experimental scenarios will be provided, which is also hoped to be useful for the nonspecialist and, in particular, promote discussions between theorists and experimentalists.

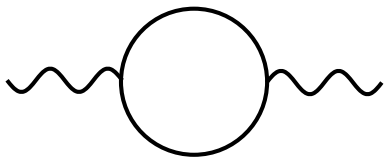

Figure 1. Vacuum polarization loop in QED. Wavy and straight lines represent photons and fermions (electrons and positrons), respectively.

2. Introduction: vacuum polarization

Vacuum polarization, depicted in the Feynman diagram of Figure 1, is a basic radiative correction that modifies the propagation of photons in vacuum through the appearance of virtual pairs in a 'fermion loop'.

There are two complementary interpretations of this effect. The first is based on what is called 'old-fashioned' perturbation theory which emphasizes energy considerations at the price of manifest covariance[8]. In this interpretation, Heisenberg's uncertainty relation is invoked to show how quantum mechanics predicts energy and momentum conservation may be violated. The amount of this violation is inversely proportional to the space–time scale over which it occurs. This effect is represented by short-lived 'virtual' particles. The second, equivalent interpretation is manifestly covariant and regards the virtual pairs as quantum

Correspondence to: B. King, Centre for Mathematical Sciences, Plymouth University, Plymouth PL4 8AA, United Kingdom. Email: b.king@plymouth.ac.uk

fluctuations. In this interpretation, at any space–time point there is a nonvanishing probability amplitude for a photon to fluctuate into a pair (or a pair and a photon or in fact any number of particles allowed by the original photon quantum numbers). In this view, energy–momentum conservation is not violated, but the virtual particles do not obey Einstein's famous equation relating energy and mass.

The main physical effect of vacuum polarization is charge renormalization due to polarization screening as explained in any standard quantum field theory text[9]. The electric charge of a particle increases as one 'dives' into its virtual polarization cloud, hence with decreasing distance from the particle. As a result, the electric charge becomes scale-dependent which may be expressed in terms of a distance-dependent fine structure constant, $\alpha = \alpha(R)$. At distances large compared to the electron Compton wavelength, $R = \lambda\!\!\!^{-}_e = \hbar/mc$, the typical length scale of QED, one has $\alpha = e^2/4\pi\hbar c \simeq 1/137$. However, at the much smaller Compton wavelength of, say, the Z boson, $R = \lambda\!\!\!^{-}_Z = \hbar/M_Z c$, the QED coupling α increases to $\alpha(\lambda\!\!\!^{-}_Z) \simeq 1/128$.

At typical laser energies, the dominant screening particles are indeed pairs of virtual electrons and positrons. Their (virtual) presence may be probed by coupling them to additional photons (see Figure 2), which may represent either fluctuating quantum fields or classical background fields such as provided by lasers. In either case, we are led to consider the probing of vacuum polarization by 'photon–photon scattering'. When large numbers of photons are involved, a classical metaphor of this quantum effect is of charged vacuum pairs forming a polarizable 'vacuum plasma' medium with a nonlinear susceptibility and permeability. An important consequence of this quantum correction to Maxwell's equations is the violation of the principle of superposition for electromagnetic waves in vacuum.

3. Analytical methods

The microscopic theory describing laser–matter or laser–laser interactions is QED described by the Lagrangian

$$\mathcal{L}_{\mathrm{QED}} = \bar\psi(\mathrm{i}\partial\!\!\!/ - m)\psi - \tfrac{1}{4}F_{\mu\nu}F^{\mu\nu} - e\bar\psi A\!\!\!/\psi, \qquad (1)$$

the separate terms representing the Dirac, Maxwell and interaction Lagrangians, respectively. The latter derives from 'minimal substitution', that is the replacement of the ordinary by the covariant derivative, $\mathrm{i}\partial \to \mathrm{i}\partial - eA \equiv \mathrm{i}D_A$ in the free Dirac term, which leads to the usual coupling of the photon field A_μ to the Dirac current $j^\mu = e\bar\psi\gamma^\mu\psi$ as $e\bar\psi A\!\!\!/\psi = A_\mu j^\mu$. An intense laser field will normally be included as a classical, external background field A_{ext} by the prescription of replacing $A \to A + A_{\mathrm{ext}}$ in the interaction term only. This guarantees that A_{ext} is not altered by the interaction because the Maxwell term will only contain the field strength tensor built from the fluctuating fields A_μ, i.e., $F_{\mu\nu} = \partial_\mu A_\nu - \partial_\nu A_\mu$.

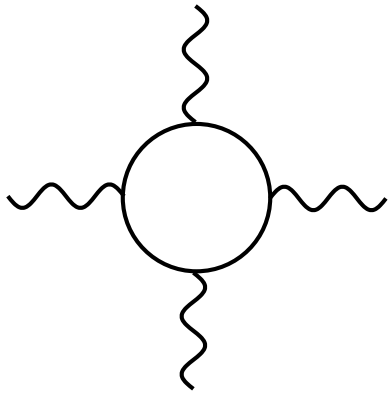

Figure 2. Probing vacuum polarization by photon–photon scattering.

In this contribution we are interested in laser–laser interactions. In this case, the centre-of-mass energy (even for x-rays) will always be much lower than the electron rest energy, mc^2. It is thus sufficient to work with the low-energy effective field theory obtained from the QED Lagrangian by 'integrating out' the Dirac fields. This can be done by employing the functional integral representation of the QED vacuum persistence amplitude Z relating in and out vacua:

$$\begin{aligned} Z &= \int \mathcal{D}A\,\mathcal{D}\psi\,\mathcal{D}\bar\psi\,\exp(\mathrm{i}S_{\mathrm{QED}}[A,\psi,\bar\psi]) \\ &\equiv \int \mathcal{D}A\,\exp(\mathrm{i}S_{\mathrm{eff}}[A]). \end{aligned} \qquad (2)$$

In the second step, the fermionic degrees of freedom have been integrated out by performing a Gaussian integral resulting in a fermionic determinant,

$$\exp(\mathrm{i}S_{\mathrm{eff}}[A]) = \exp\left(\mathrm{Tr}\ln\frac{\mathrm{i}D\!\!\!/_A - m}{\mathrm{i}\partial\!\!\!/ - m}\right), \qquad (3)$$

where we have re-exponentiated using $\mathrm{Det} = \exp\mathrm{Tr}\ln$. The fermionic determinant depends on the photon field A and can only be evaluated analytically for special configurations such as constant fields. Alternatively, one may perform a derivative (i.e., low-energy) expansion[10, 11], the leading order of which coincides with the constant field evaluation. For QED this has been done long ago (using different techniques)[12–14], the result being the celebrated Heisenberg–Euler Lagrangian

$$\begin{aligned} \mathcal{L}_{\mathrm{HE}} = -\frac{m^4}{8\pi^2}\int_0^\infty \mathrm{d}s\,\frac{\exp(-s)}{s^3} \\ \times\left[s^2 ab\cot as\,\coth bs - 1 + \frac{s^2}{3}(a^2-b^2)\right], \end{aligned} \qquad (4)$$

https://doi.org/10.1017/hpl.2016.1 Published online by Cambridge University Press

where the dimensionless secular invariants a and b are given by:

$$a = \frac{[\sqrt{\mathcal{F}^2 + \mathcal{G}^2} + \mathcal{F}]^{1/2}}{E_{\rm cr}}; \quad b = \frac{[\sqrt{\mathcal{F}^2 + \mathcal{G}^2} - \mathcal{F}]^{1/2}}{E_{\rm cr}}.$$

These contain the two electromagnetic invariants

$$\mathcal{F} = -F_{\mu\nu}F^{\mu\nu}/4 = (E^2 - B^2)/2, \tag{5}$$
$$\mathcal{G} = -F^{\mu\nu}\tilde{F}_{\mu\nu}/4 = \mathbf{E}\cdot\mathbf{B} = 0, \tag{6}$$

with field and dual field strength tensors, electric and magnetic fields ($F^{\mu\nu}$, $\tilde{F}^{\mu\nu}$, $\mathbf{E}$ and $\mathbf{B}$, respectively) and the critical field strength:

$$E_{\rm cr} = \frac{m^2c^3}{e\hbar} \equiv \frac{m^2}{e}. \tag{7}$$

(Note that we now adopt natural units, $\hbar = c = 1$, for the remainder of this section unless otherwise explicitly stated.) The critical, 'Sauter'[15] or 'Schwinger'[14] field strength $E_{\rm cr}$ is built from the fundamental constants of QED and is the typical field-scale separating weak ($E \ll E_{\rm cr}$) from strong-field ($E > E_{\rm cr}$) vacuum polarization phenomena.

The Heisenberg–Euler Lagrangian (Equation (4)) is equivalent to QED for arbitrary values of the field strength but at energies small compared to mc^2. For the foreseeable future, laser experiments will stay well below the critical field strength, hence in the weak-field limit. Thus, to a very good approximation, it is sufficient to work with the leading order in a field strength expansion of Equation (4) given by:

$$\mathcal{L}^{(2)}_{\rm HE} \simeq c_1\mathcal{F}^2 + c_2\mathcal{G}^2, \tag{8}$$

with dimensionless low-energy constants

$$\begin{Bmatrix} c_1 \\ c_2 \end{Bmatrix} = \frac{2\alpha^2}{45m^4}\begin{Bmatrix} 4 \\ 7 \end{Bmatrix}. \tag{9}$$

These define effective vertices corresponding to the low-energy limit of the diagram in Figure 2 with the fermion loop no longer being resolved, see Figure 3.

The cross-section for the low-energy limit of real photon–photon scattering depicted in Figure 3 is given by[16]:

$$\sigma = \frac{973}{10125\pi}\alpha^4\left(\frac{\omega}{m}\right)^6 \lambda\!\!\!^{-2}_e\left[1 + \frac{640}{2919}\left(\frac{\omega}{m}\right)^2\right]; \quad \omega \ll m$$

whereas the high-energy limit is given by[17–19]:

$$\sigma = 4.7\,\alpha^4\left(\frac{m}{\omega}\right)^2 \lambda\!\!\!^{-2}_e; \quad \omega \gg m.$$

The maximum of the cross-section is at the pair-creation threshold of colliding photon centre-of-mass energies $\omega = m$.

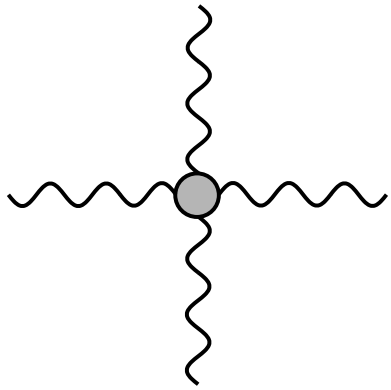

Figure 3. The leading-order Heisenberg–Euler vertex or photon–photon scattering at low energies.

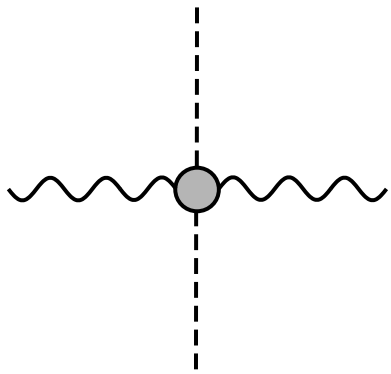

Figure 4. A probe photon (wavy lines) scattering off a classical laser background (dashed lines) at low energy (so that the Heisenberg–Euler vertex can be employed).

3.1. Scattering matrix

In what follows, we will consider a modification of the 4-photon scattering amplitude at low energy by assuming that two of the photons involved are stemming from a high-intensity laser which is probed by a dynamical photon 'passing through'. This is visualized in Figure 4.

We assume that an incoming probe photon with four-momentum k and four-polarization ε scatters off a laser background described by a field strength tensor $F_{\mu\nu}$ resulting in an outgoing photon with quantum numbers k' and ε'. The resulting scattering amplitude is given by the S-matrix element

$$\langle \varepsilon', k'; \text{out}|\varepsilon, k; \text{in}\rangle = \langle \varepsilon', k'|\hat{S}|\varepsilon, k\rangle \equiv S_{\rm fi}(\varepsilon', k', \varepsilon, k). \tag{10}$$

Using the leading-order Lagrangian (Equation (8)), using $S_{\rm fi}(q)$ to denote $S_{fi}(\varepsilon', k', \varepsilon, k)$, the S-matrix element takes on the simple form of a Fourier integral

$$S_{\rm fi}(q) = -\mathrm{i}\int d^4x\, \mathrm{e}^{\mathrm{i}q\cdot x}\, S_{\rm fi}(x), \tag{11}$$

https://doi.org/10.1017/hpl.2016.1 Published online by Cambridge University Press

where $q = k' - k$ is the momentum transfer and

$$S_{\mathrm{fi}}(x) = c_1(k', F\varepsilon')(k, F\varepsilon) + c_2(k', \tilde{F}\varepsilon')(k, \tilde{F}\varepsilon), \quad (12)$$

employing the abbreviated scalar products $(k, F\varepsilon) \equiv k_\mu F^{\mu\nu}\varepsilon_\nu$, etc. Hence, one may introduce an *intensity form factor*,

$$W^{\mu\alpha,\nu\beta}(q) \equiv -\mathrm{i}\int d^4x\, \mathrm{e}^{\mathrm{i}q\cdot x}(c_1 F^{\alpha\mu}F^{\beta,\nu} + c_2\tilde{F}^{\alpha\mu}\tilde{F}^{\beta,\nu}), \quad (13)$$

which is the Fourier transformation of the background intensity distribution. In terms of the latter, the scattering amplitude may be written as

$$S_{\mathrm{fi}}(q) = \varepsilon'_\alpha k'_\mu W^{\mu\alpha,\nu\beta}(q) k_\nu \varepsilon_\beta. \quad (14)$$

The results above are reminiscent of elastic electron nucleus scattering, where the scattering amplitude is proportional to the nuclear charge form factor which is nothing but the Fourier transform of the nuclear charge distribution. In photon–photon scattering, one is naturally probing an intensity, rather than a charge, distribution. To proceed, one has to choose a suitable laser background field, $F_{\mu\nu}(x)$, and calculate its intensity form factor (Equation (13)).

3.2. Polarization operator

An equivalent representation is obtained in terms of a quantity aptly called the polarization operator, denoted $\Pi^{\mu\nu}$. In its simplest incarnation it is just the mathematical expression for the Feynman diagram of Figure 1, namely

$$\Pi^{\mu\nu} = -\mathrm{i}e^2\,\mathrm{tr}_\gamma \int \frac{d^4p}{(2\pi)^4}\gamma^\mu \frac{1}{\not{p} - m}\gamma^\nu \frac{1}{(\not{p} - \not{k} - m)}, \quad (15)$$

where the trace tr_γ extends over the Dirac matrices γ^μ. One may generalize this to the polarization tensor in an external field A_{ext}, where one trades the free fermion propagators for interacting ones through the standard minimal substitution $p \to p - eA_{\mathrm{ext}}$. Indeed, this method has a long history[20–23] as reviewed by Ref. [24]. For our purposes it is sufficient to just employ the first-order weak-field Heisenberg–Euler Lagrangian (Equation (8)) once again and rewrite it as

$$\mathcal{L}^{(2)}_{\mathrm{HE}} = \tfrac{1}{2} A_\mu \Pi^{\mu\nu}[A_{\mathrm{ext}}]A_\nu, \quad (16)$$

with the polarization tensor thus defining the second-order term. From Equation (8) one can straightforwardly read off that

$$\Pi^{\mu\nu}[A_{\mathrm{ext}}] = \frac{c_1}{2}k_\alpha F^{\alpha\mu}F^{\beta\nu}k_\beta + \frac{c_2}{2}k_\alpha \tilde{F}^{\alpha\mu}\tilde{F}^{\beta\nu}k_\beta, \quad (17)$$

where the background field strength $F^{\mu\nu} = \partial^\mu A^\nu_{\mathrm{ext}} - \partial^\nu A^\mu_{\mathrm{ext}}$.

To connect this approach with the S matrix formalism we specialize to forward scattering by setting $k = k'$ in Equation (12) which yields the relation

$$S_{\mathrm{fi,fwd}}(k) = \varepsilon'_\mu(k)\Pi^{\mu\nu}(k)\varepsilon_\nu(k). \quad (18)$$

This makes the link between the polarization operator and scattering matrix approaches manifest.

3.3. Modified Maxwell equations

In standard quantum field theory notion[9], the total Heisenberg–Euler action, $S_{\mathrm{eff}} = \int d^4x\, \mathcal{L}_{\mathrm{eff}}$, is nothing but the one-loop effective (or quantum) action of QED evaluated at low energies where there are no external electron lines. The associated effective Lagrangian is the sum of the classical Maxwell term $\mathcal{L}_{\mathrm{M}} = (E^2 - B^2)/2$ and the first quantum correction:

$$\mathcal{L}_{\mathrm{eff}} = \mathcal{L}_{\mathrm{M}} + \mathcal{L}_{\mathrm{HE}}. \quad (19)$$

By variation of the quantum action, one can derive the corresponding modified Maxwell equations[25]:

$$\boldsymbol{\nabla}\cdot\mathbf{E} = \rho_{\mathrm{vac}}; \quad \boldsymbol{\nabla}\wedge\mathbf{B} = \mathbf{J}_{\mathrm{vac}} + \partial_t\mathbf{E}, \quad (20)$$

in which:

$$\rho_{\mathrm{vac}} = \boldsymbol{\nabla}\cdot\mathbf{P}_{\mathrm{vac}}; \quad \mathbf{J}_{\mathrm{vac}} = \boldsymbol{\nabla}\wedge\mathbf{M}_{\mathrm{vac}} + \partial_t\mathbf{P}_{\mathrm{vac}} \quad (21)$$

and the vacuum polarization and magnetization are:

$$\mathbf{P}_{\mathrm{vac}} = \frac{\partial\mathcal{L}_{\mathrm{HE}}}{\partial\mathbf{E}}; \quad \mathbf{M}_{\mathrm{vac}} = \frac{\partial\mathcal{L}_{\mathrm{HE}}}{\partial\mathbf{B}}. \quad (22)$$

The wave equations:

$$\partial_t^2\mathbf{E} - \boldsymbol{\nabla}^2\mathbf{E} = -\boldsymbol{\nabla}\rho_{\mathrm{vac}}[\mathbf{E},\mathbf{B}] - \partial_t\mathbf{J}_{\mathrm{vac}}[\mathbf{E},\mathbf{B}], \quad (23)$$

$$\partial_t^2\mathbf{B} - \boldsymbol{\nabla}^2\mathbf{B} = \boldsymbol{\nabla}\wedge\mathbf{J}_{\mathrm{vac}}[\mathbf{E},\mathbf{B}], \quad (24)$$

can be solved using, for example, the method of Green's functions.

4. Signatures of vacuum polarization

The most general vacuum polarization diagram represents an elastic scattering amplitude that relates an incoming ensemble of photons $|k_1, \ldots, k_n\rangle$, which interact in some experimental scenario, to an outgoing ensemble of photons $|k'_1, \ldots, k'_{n'}\rangle$. In this review, we concentrate on processes that could be measured using high-power lasers. The fields of these lasers are included in calculations in various ways. A 'monochromatic plane wave' will refer to an infinitely

https://doi.org/10.1017/hpl.2016.1 Published online by Cambridge University Press

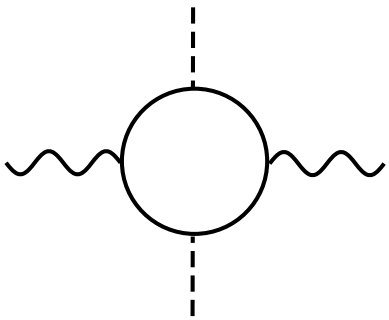

Figure 5. Photons from the pump (dashes) interact with those from the probe to produce a pump-dependent vacuum index of refraction.

extended wave with no transverse structure, a 'beam' will refer to some inclusion of structure, e.g., a cylinder of radiation is a 'beam', a 'focused beam' will imply some approximation to a real beam with focal width as a parameter and a 'pulse' to a field localized in time with pulse duration as a parameter. Since laser pulse wavelengths are much larger than the Compton wavelength, and since expected electric field strengths are much less than the critical Sauter field, equivalent to an intensity of the order of 10^{29} W cm^{-2}, the interaction of laser pulses with virtual electron–positron pairs can be expanded in terms of weak fields. Starting at $n = 2$ as in Equation (8), each perturbative order describes a vacuum $2n$-wave mixing process. It is noteworthy that unlike when real electrons and positrons interact with intense laser fields, for virtual electron–positron pairs, the number of laser photons involved is typically small[26], which is why the discussion is mostly in terms of four-wave mixing processes such as in Figure 5. This means the vacuum is often compared to a nonlinear optical material with a Kerr-like response[27]. Although there is a large overlap with nonlinear optics, a major difference is the way the polarization of the dielectric (here, the vacuum) can be shaped by the pump laser pulse.

The majority of suggested signals of vacuum polarization can be described by considering how the photons from a probe laser change due to interaction with a more intense pump laser. The pump laser will also be referred to as the 'background' or the 'strong field' where appropriate. The probe laser quantities will often be denoted with subscript p and the pump or strong laser quantities with the subscript s. The source of probe photons will mostly be a high-power laser, which, satisfying $E/E_{\rm cr} \gg \sqrt{\alpha}(\omega/m)^2$, often allows the external field concept to be invoked for the probe[28]. Therefore, the discussion will include interchangeably effects on probe photons and on the probe electromagnetic field, which assumes the photon-scattering process can be summed incoherently over the probe photon distribution. We begin by reviewing the consequence of real photon–photon scattering at the level of probe laser photons:

$$\gamma(\omega, \mathbf{k}, \varepsilon(k)) \to \gamma(\omega', \mathbf{k}', \varepsilon'(k')). \tag{25}$$

Three measurable quantities have been highlighted – the effect on the probe's frequency ω, its wavevector $\mathbf{k}$ and its polarization $\varepsilon(k)$ and these will be discussed in turn.

4.1. Effects on probe photon polarization

Vacuum birefringence refers to the prediction that the refractive index experienced by a probe propagating through regions of intense, but weakly varying strong fields of amplitude E_s is of the form[20, 29]:

$$\mathsf{n}_{\rm vac}^{\parallel,\perp} = 1 + \frac{(11 \mp 3)\alpha}{45\pi}\frac{E_s^2}{E_{\rm cr}^2}, \tag{26}$$

where the $\parallel$ ($\perp$) indices apply to a probe polarized parallel (perpendicular) to the strong background. This result may be derived from the Heisenberg–Euler quantum equation of motion,

$$(\partial_\lambda \partial^\lambda g^{\mu\nu} - \partial^\mu \partial^\nu + \Pi^{\mu\nu})A_\nu = 0. \tag{27}$$

A plane-wave ansatz for A_ν implies *two* secular equations or dispersion relations,

$$k^2 - \Pi_{1,2}(k) = (g^{\mu\nu} - c_{1,2}T^{\mu\nu})k_\mu k_\nu = 0, \tag{28}$$

where $\Pi_{1,2} = c_{1,2}(k, Tk)$ are the two nontrivial eigenvalues of the polarization tensor (Equation (17)), expressed in terms of the background energy–momentum tensor $T^{\mu\nu} = F_\alpha^\mu F^{\alpha\nu}$. The dispersion relations (Equation (28)) describe the change in light propagation caused by the energy–momentum density stored in the background field and have been referred to as modified light-cone conditions[30, 31]. They imply group velocities different from the vacuum speed of light, c, and hence the refractive indices (Equation (26)) different from unity, which can be rewritten as $\mathsf{n}_{\rm vac}^{\parallel,\perp} = 1 + \Pi_{1,2}/2\omega_p^2$, $\omega_p = k^0 c$ being the probe frequency.

The result for the refractive indices has been shown to hold to all perturbative orders using the polarization operator[20, 31, 32] and Heisenberg–Euler Lagrangian numerically[33, 34] and analytically[34]. When the pump field is space–time-dependent as is the case for laser pulses, the effect on the probe is calculated by integrating over the inhomogeneous refractive index of the pump background[35]. There has also been recent work indicating finite-time effects in an inhomogeneous background may leave a detectable signal[36].

Polarization flip is the underlying physical mechanism of vacuum birefringence. The term is used when an incoming photon's polarization vector ε^μ is 'flipped' to an orthogonal one ε'^μ due to real photon–photon scattering. Linearly polarized probe photons can flip if the background contains some ellipticity and circularly polarized probe

https://doi.org/10.1017/hpl.2016.1 Published online by Cambridge University Press

photons if the background contains some linear polarization. The flip amplitude (for a head-on collision of probe and background) after a propagation distance z can be found from the Heisenberg–Euler forward scattering amplitude (Equation (18)) and coincides with the birefringence-induced ellipticity[37],

$$\mathsf{e} \equiv \langle \varepsilon', k|S|\varepsilon, k\rangle = 2E_s^2\omega_p z(c_2 - c_1), \tag{29}$$

where $\varepsilon \cdot \varepsilon' = 0$. Note the dependence on the *difference* of the low-energy constants. This implies that a confirmation of vacuum birefringence would rule out other versions of electrodynamics popular in beyond-the-standard-model physics such as Born–Infeld theory, which has $c_1 = c_2$[38–40]. From Equation (26), the flip amplitude or ellipticity (Equation (29)) has the equivalent representation

$$\mathsf{e} = \omega_p z \frac{\mathsf{n}_{\rm vac}^{\perp} - \mathsf{n}_{\rm vac}^{\parallel}}{2}, \tag{30}$$

which is proportional to the difference in refractive indices, hence the phase shift between different polarizations.

Detailed calculations have been performed for photons propagating in an arbitrary plane-wave background[22, 37], and the kinematic low-energy limit relevant for laser-based experiments was found to be consistent with use of the Heisenberg–Euler approach for calculating birefringence and ellipticity[41]. A study of the dependency of the flip and nonflip amplitude on spatial and timing jitter and angle of incidence[42] was performed, with the results also being consistent with a previous similar study in the low-energy limit[43]. Both studies[42, 43] found that modelling the background as a focused paraxial Gaussian beam without taking into account the finite pulse duration led to an order of magnitude discrepancy in the number of scattered photons.

Induced ellipticity is a consequence of birefringence as pointed out in the previous subsection, see Equations (29) and (30). The polarization of a linearly polarized probe plane wave can be described with the vector:

$$\begin{pmatrix} \varepsilon^{\parallel} \\ \varepsilon^{\perp} \end{pmatrix} = \cos\varphi \begin{pmatrix} \cos\theta \\ \sin\theta \end{pmatrix}, \tag{31}$$

where φ is the probe phase. If, over some probe phase $\omega_p z$ the $\parallel$ and $\perp$ components experience a different refractive index, then when the phase shift $\delta\varphi^{\parallel,\perp} = n^{\parallel,\perp}\omega_p z \ll 1$, the polarization changes to:

$$\begin{pmatrix} \varepsilon^{\parallel} \\ \varepsilon^{\perp} \end{pmatrix} = \begin{bmatrix} \cos\theta & -\cos\theta\ \delta\varphi^{\parallel} \\ \sin\theta & -\sin\theta\ \delta\varphi^{\perp} \end{bmatrix} \begin{pmatrix} \cos\varphi \\ \sin\varphi \end{pmatrix}, \tag{32}$$

and the originally linearly polarized probe is now elliptically polarized. If the background is constant, the ellipticity can be written[44]:

$$\mathsf{e} = \omega_p z \frac{\mathsf{n}_{\rm vac}^{\perp} - \mathsf{n}_{\rm vac}^{\parallel}}{2} \sin 2\theta, \tag{33}$$

which generalizes Equation (30). The induced ellipticity in the interaction of an x-ray probe plane wave of wavelength $\lambda_p = 0.4$ nm counterpropagating with a Gaussian pump beam of intensity 10^{23} W cm^{-2} and wavelength $\lambda_s = 745$ nm focused to 8 μm was calculated[44] to experience an ellipticity of $\mathsf{e} \approx 5\times10^{-9}$ rad when measured at a distance of 0.25 m from the pump–probe collision. By considering the same pump energy distributed over two pump Gaussian laser beams counterpropagating with a Gaussian probe beam, a modest improvement of around $\sqrt{2}$ was found, and the near-field-induced ellipticity[45]

$$\mathsf{e} = \frac{2\pi\alpha}{15}\frac{I_s}{I_{\rm cr}}\frac{z_{\rm eff.}}{\lambda_p}\sin 2\theta; \quad z_{\rm eff.} = \frac{z_{r,p}z_{r,s}}{z_{r,p} + z_{r,s}}, \tag{34}$$

with the effective interaction length between the two Gaussians $z_{\rm eff.}$ depending on the probe $z_{r,p}$ and pump $z_{r,s}$ Rayleigh lengths. This agrees with the expressions calculated for a monochromatic probe plane wave counterpropagating with a Gaussian pump[46] in the limit $z_{r,p} \to \infty$.

Polarization rotation is the macroscopic consequence of coherent polarization flipping at the photon level. The effect on the transverse photon polarization states in Equations (31) and (32) has the consequence that the polarization angle θ will rotate as the initially linearly polarized probe acquires an ellipticity. The ellipse traced out by the probe field vector can be seen to be[47]:

$$x^2 - 2xy\cos(\delta\varphi^{\perp} - \delta\varphi^{\parallel}) + y^2 = \sin^2(\delta\varphi^{\perp} - \delta\varphi^{\parallel}), \tag{35}$$

where $x\cos\theta = \varepsilon^{\parallel}$ and $y\sin\theta = \varepsilon^{\perp}$. For an x-ray probe counterpropagating with an optical Gaussian pump beam, the rotation angle was found to be the same order of magnitude as the induced ellipticity[44, 45].

4.2. Effects on probe photon wavevector

On the photon level, four-wave mixing as depicted in Figure 5 can be understood as two incoming photons, one from the probe and one from the pump, being scattered to two outgoing photons, one being back into the pump field and the other being the signal of the vacuum interaction. Conservation of momentum permits the scattered photons having a wider transverse distribution than the probe and strong background, hence allowing one to spatially separate the photon–photon scattering signal from the large background of pump and probe laser photons.

On the classical level, a refractive index $\mathsf{n}_{\rm vac}$ different from unity, implies altered transmitted wavevectors via Snell's law, and altered transmission T and reflection coefficient R

https://doi.org/10.1017/hpl.2016.1 Published online by Cambridge University Press

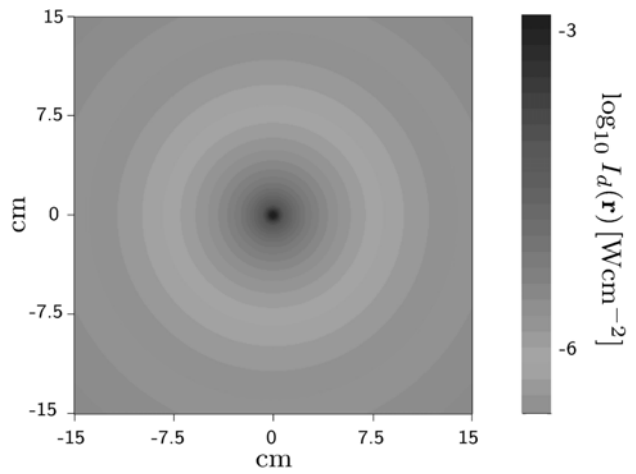

Figure 6. Predicted diffracted electric field in a collision of two counterpropagating Gaussian beams. Adapted from [47].

via Fresnel's law at perpendicular incidence[48]:

$$T = \frac{4\,\mathsf{n}_{\rm vac}}{(1+\mathsf{n}_{\rm vac})^2}; \quad R = \left(\frac{1-\mathsf{n}_{\rm vac}}{1+\mathsf{n}_{\rm vac}}\right)^2. \tag{36}$$

If the vacuum refractive index is written as $\mathsf{n}_{\rm vac} = 1+\delta\mathsf{n}_{\rm vac}$, the effect on probe transmission $\sim O(\delta\mathsf{n}_{\rm vac})$ whereas the effect on reflection $\sim O(\delta\mathsf{n}^2_{\rm vac})$.

If the probe beam is considered to be much wider than the pump background, the region of polarized vacuum can be considered to 'diffract' the probe. An example of such a 'single-slit' diffraction pattern is given in Figure 6. It is well known that the far-field diffracted field is related to the Fourier transform of the aperture function[49], and via Babinet's principle, this can be related to an integral over the region of refractive index different from unity. We underline the connection of this classical analogue to the intensity form factor of the scattering matrix approach Equation (13).

Vacuum diffraction was considered in the collision of a plane probe and a focused Gaussian pump beam[44], and extended to the collision of focused Gaussian probe and pump beams[50]. The advantage of this signal is that for increasing scattering angle, while the focused laser background is exponentially suppressed, the scattered photon vacuum signal is power-law suppressed. In the detector plane then, the number of scattered photons can be calculated in 'measurable' regions, where the signal-to-noise ratio is much larger than unity. One interesting scenario was calculated of colliding two parallel, highly focused Gaussian pump beams with a wide weakly focused Gaussian probe beam, such that the photons scattered in the two slit-like polarized regions around the pump beams would interfere and hence together form an all-optical double-slit experiment[50]. For the case of two colliding Gaussian pulses, the dependency of the diffracted photon signal on experimental parameters such as the total beam power, spatial and timing jitter, angle of collision, pulse duration, probe wavelength and focal width has been carried out[43]. With 10 PW total laser power split into pump and probe focused optical pulses, of the order of a few photons were predicted to be diffracted into measurable regions on a detector place 1 m from the interaction centre. These results were verified in a study by different authors[51], who used a different beam model. The diffraction paradigm was extended from single and double slits to a 'diffraction grating' of having a probe beam diffract off a regular series of pump beams[52]. Only on positions of the detector where the Bragg condition:

$$nq = 2k_p \sin\frac{\theta}{2},$$

for integer n, probe wavenumber k_p, wavenumber of the pump beam structure q and angle between incoming and diffracted probe θ, is there constructive interference of the signal of scattered photons. Since the addition of diffracted waves occurs at the level of the field, and since the number of photons scattered depends upon the total diffracted field squared, there is an enhancement in such a setup proportional to the square of the number of modulation periods. Alternatively, rather than using many beams, a single, wide-angle beam diffracting with itself at the focus has also been studied[53], with the conclusion that the number of diffracted photons increases exponentially with the angular aperture. Since only the near-field signal was presented, more work is required to determine measurability in this scheme.

The idea of using the diffracted photons' flipped polarization as well as their altered wavevector in an experimental measurement was explored for the wide-angled single-beam setup[53], a single propagating Gaussian beam taking into account higher orders in a Hermite–Gauss expansion[54] and has been most recently applied to the upcoming HIBEF experiment[55].

Vacuum reflection refers to the back-scattering of photons in real photon–photon scattering. Static magnetic inhomogeneities of the form of a Lorentzian, Gaussian and oscillating Gaussian have been studied[56] and more recently static electromagnetic inhomogeneities but most significantly scattering in a Gaussian beam[57], although calculations for pulses of a finite duration are still to be performed.

4.3. Effects on probe photon frequency

The frequency of probe photons can change via interaction with the polarized vacuum. However, this effect is much more difficult to measure experimentally because of the limited range of energy and momenta for which it is permitted. Suppose via the four-photon interaction, two

https://doi.org/10.1017/hpl.2016.1 Published online by Cambridge University Press

Figure 7. Parametric frequency upshifting (left) and downshifting (right) can occur between pump and probe through the vacuum interaction.

photons from the strong pump background merge with a probe photon as depicted in Figure 7. Then via energy–momentum conservation:

$$\omega_p + \omega_{s,1} + \omega_{s,2} = \omega'; \quad \mathbf{k}_p + \mathbf{k}_{s,1} + \mathbf{k}_{s,2} = \mathbf{k}', \qquad (37)$$

but at the same time, the photon must be real to propagate to the detector so $\omega'^2 = \mathbf{k}' \cdot \mathbf{k}'$. This constrains the allowed frequencies, momenta and angles that can be combined. Similar relations occur for Raman and Brillouin scattering[58], except all the waves here are electromagnetic.

Vacuum parametric frequency shifting has been calculated for special beam configurations. Combining three monochromatic plane waves at right angles, whose wavelengths are 800, 800 and 400 nm, was predicted to produce a signal that is spatially and frequentially (at 267 nm) separated from the background[59]. For respective beam powers 0.1, 0.1 and 0.5 PW, taking the interaction region to be cuboidal, on average 0.07 photons would be frequency-upshifted per collision of the beams, which is predicted to be larger than the Compton-scattering background. A signature of the frequency-shifting four-wave mixing process on the number of total measurable diffracted photons for a collision of two ultra-short focused Gaussian pulses was also calculated[43]. For 10 PW total beam power split into a probe with wavelength 228 nm and duration 2 fs, as the duration of the 910 nm pump is reduced to 1 fs, the total number of diffracted photons is predicted to change by around 20%, equal to one photon per shot. Calculations beyond the paraxial approximation recently performed[60] for two co-propagating beams of different frequencies incident on a parabolic mirror suggest 1–10 PW laser beams are required to observe vacuum frequency mixing, although the method of detecting the signal needs to be given more attention.

Vacuum high-harmonic generation can take place if the colliding laser pulses have the same frequency. Then via the four-wave mixing process in Equation (37), if $\omega_p = \omega_{s,1} = \omega_{s,2} = \omega$, the signal of the vacuum process has a frequency $\omega' = 3\omega$ and so is at the third harmonic of the probe. By considering six-, eight- and in general $2n$-wave mixing as depicted in Figure 8, it can be seen that a harmonic spectrum for the vacuum interaction can be produced. As each extra interaction between the virtual pair and a laser photon is weighted at the amplitude level with a factor $E/E_{\rm cr} \ll 1$,

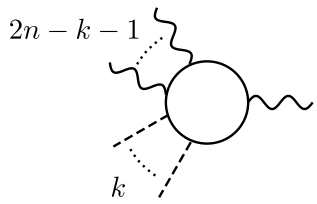

Figure 8. Vacuum high-harmonic generation of the nth harmonic of the probe via $2n$-photon scattering.

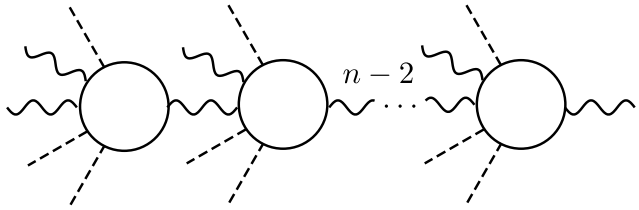

Figure 9. Vacuum high-harmonic generation of the nth harmonic of the probe via a chain of six-photon scattering.

higher harmonics are in general exponentially suppressed. Nevertheless, the harmonic spectrum produced by a standing wave formed of two monochromatic pump laser beams was calculated for subcritical ($E < E_{\rm cr}$) strengths where higher harmonic orders j were found[61] to follow the hierarchy $(E/E_{\rm cr})^{4j}$. In a setup involving three beams, the minimum power of each laser required to scatter one photon was found to be:

$$P_{\rm min} \approx 33.5 \, \frac{\lambda}{1\ {\rm nm}} \frac{w_0}{1\ {\rm nm}} \left(\frac{1\ {\rm fs}}{\tau}\right)^{1/3} \left(\frac{1\ {\rm fs}}{\tau_c}\right)^{2/3} {\rm GW}, \qquad (38)$$

for typical beam cross-sectional dimension w_0, interaction duration τ and coherence time τ_c. The most likely frequency of the scattered photon is, however, the fundamental harmonic. The intensity at which a single focused laser pulse will begin to produce harmonics via self-interaction has been studied[62], with the conclusion that a pulse of 1000 nm photons focused within a cone of angle 0.1 rad will produce one photon per period at 5×10^{27} W cm^{-2}. A recent calculation of an alternative route to high-harmonic generation through having many scattering events involving low numbers of photons[63–68] (as in Figure 9) has recently been suggested to be more efficient. For the collision of a Gaussian probe at much higher frequency than the background, if the parameter $(64\alpha/105\pi)(E_s^3 E_p/E_{\rm cr}^4)\omega_p \tau_s$, where τ_s is the duration of the pump, can be made close to unity, harmonic generation will dominate, with the spectrum displaying a power-law behaviour and the appearance of a corresponding electromagnetic shock[34].

Photon splitting as depicted in Figure 10, is sometimes thought of as the opposite of high-harmonic generation, but unlike harmonic generation, the emitted photons can have a continuum of energies. If one considers splitting

https://doi.org/10.1017/hpl.2016.1 Published online by Cambridge University Press

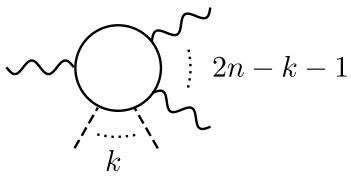

Figure 10. An incoming probe photon can split into k outgoing ones, due to interaction with the background.

to two photons via four-wave mixing then via energy and momentum conservation, one possibility is:

$$\omega_p + \omega_s = \omega_1' + \omega_2'; \quad \mathbf{k}_p + \mathbf{k}_s = \mathbf{k}_1' + \mathbf{k}_2', \qquad (39)$$

where now two constraints on these equations are $(\omega_{1,2}')^2 = \mathbf{k}_{1,2}' \cdot \mathbf{k}_{1,2}'$. The continuum of allowed energies and the possibility for a wide angular distribution of emitted photons makes this process worthy of study. The process has been comprehensively studied for a probe photon propagating through a plane-wave background of arbitrary form and polarization[69], which was found to depend on the two parameters $\eta = \omega_p\omega_s/m^2$ and $\chi = (\omega_p/m)(E/E_{\rm cr})$. Two events per hour were predicted using 10^8 250 MeV tagged photons per second almost counterpropagating with 100 fs 10^{15} W cm^{-2} 1 keV XFEL beams separated by 93 ns. Alternatively, two events per hour were also predicted using 10^8 100 MeV tagged photons counterpropagating with a 1 Hz 1 eV optical pump of intensity 10^{25} W cm^{-2}. The conclusion was that a different experimental setup must be considered if this effect is to be observed in the near future[69].

4.4. Effects on probe pulse form

In addition to the effects on single photons, one can consider the consequence of real photon–photon scattering on the propagation of an ensemble of photons. A probe laser pulse can be understood as a superposition of photons with a range of frequencies and phases. From the study of nonlinear dispersive media, it is well known that a refractive index that depends on a probe's intensity directly or indirectly can lead to pulse shape effects[58]. In particular, for the interaction with vacuum, probe pulse effects can occur if the next-to-leading-order effect of a probe-dependent refractive index is taken into account.

Nonlinear phase shift is a term used to denote the relative difference in phases between parts of a probe beam that have experienced different vacuum refractive indices. For a constant refractive index, the relative phase difference compared to a unitary refractive index is:

$$\delta\phi = (\mathsf{n}_{\rm vac} - 1)\omega_p z,$$

where $\omega_p z$ is the phase over which $\delta\phi$ has been accrued. For two counterpropagating initially monochromatic plane waves, with the envisaged ELI parameters of 800 nm wavelength, 10^{25} W cm^{-2} intensity, 10 fs duration and 10 μm focal spot diameter, a phase shift of the order of $\delta\phi \approx 10^{-7}$ rad has been calculated[33, 70]. This nonlinear phase shift can be enhanced by using multiple crossings of the interacting beams. For N_r reflections from plasma mirrors of reflectivity $R_{\rm mir}$ of two beams crossing each other at an angle θ_c, the gain factor has been calculated to be[71]:

$$\sin^4\left(\frac{\theta_c}{2}\right)\sum_{n=0}^{N_r+1} R_{\rm mir}^n.$$

The measurement of this phase shift using Fourier imaging has also been explored[72].

Vacuum self-focusing is an analogue to the well-known plasma self-focusing or 'Benjamin–Weir' instability[58] in which there is positive feedback between a refractive index increasing the intensity of a pulse via focusing, and a higher intensity resulting from that focusing in turn increasing the refractive index. Mutual channelling of counterpropagating laser pulses and large-scale focusing have been considered, but either YW powers are predicted as necessary[66] or intensities above critical[73], before which vacuum pair-creation would have set in. In considering the idealized geometry of a Gaussian plane-wave probe pulse counterpropagating and interacting via six-wave mixing with a much slower varying pump, the probe-dependent refractive index:

$$\mathsf{n}_{\rm vac}^{\parallel} = 1 + \frac{\alpha}{\pi}\frac{E_s^2}{E_{\rm cr}^2}\left[\frac{8}{45} + \frac{64}{105}\frac{E_s}{E_{\rm cr}}\frac{E_p}{E_{\rm cr}}\right] \qquad (40)$$

was predicted to lead to the generation of a shock wave, a signature of self-focusing, when the phase difference due to the probe-dependent refractive index tended to a quarter wavelength[34]. The mutual attraction between two photons due to mutual exchange of virtual photons on two vacuum loops has also been considered[74], and a self-focusing angle of $\theta = \sqrt{157/16\pi^3}(\alpha^2/180m^4R^4)$ for photon separation R.

Pulse collapse is predicted to occur for high-intensity probe pulses propagating through an even higher-intensity background. The wave equation for the probe can be recast as a nonlinear Schrödinger equation[58] with the consequence that the pulse envelope becomes space–time-dependent, even if assumed initially homogeneous. Unlike typical optically nonlinear dispersive media, the nonlinearity of the vacuum is 'formed' by the pump laser background, which is then probed by a second pulse. Even when the leading-order effect on the probe is a nonlinear refractive index that is independent of the probe pulse, because of its effect on the pump's evolution, it can indirectly effect the probe's propagation. This interplay between a Gaussian probe distribution

https://doi.org/10.1017/hpl.2016.1 Published online by Cambridge University Press

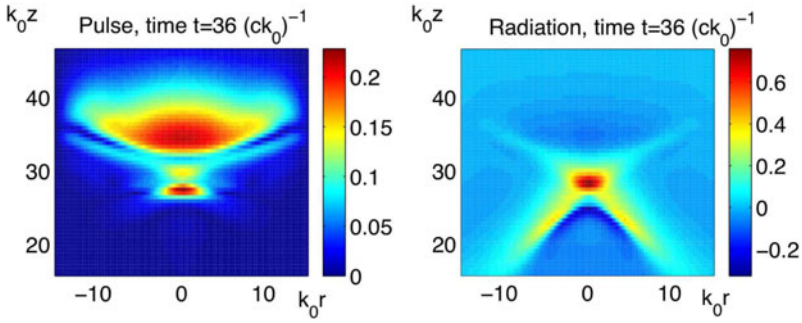

Figure 11. Cerenkov-like radiation (right) generated by pulse collapse into photon bullets (left) against longitudinal z and transverse r co-ordinates of an initially Gaussian pulse of central wavenumber k_0. Reproduced with permission[75].

propagating through a radiation gas has been demonstrated to lead to self-focusing and collapse of the probe into 'photon bullets', thereby driving acoustic waves[75] as demonstrated in Figure 11. Depending on initial parameters, probe collapse can occur before or after the critical Schwinger limit is reached[76].

4.5. Finite-time effects

Similar to the case for regular plasmas, there are effects on the probe when propagating through regions of the polarized 'vacuum plasma' that do not persist long enough to be directly detected.

Photon acceleration is well known from plasma physics[77] and corresponds to the frequency downshift (upshift) as probe photons traverse an increasing (decreasing) plasma gradient. The possibility of measuring this effect in vacuum has been considered for a probe photon propagating almost parallel with a pump pulse[78], with a frequency up (down) shift occurring at the rear (front) of the pump beam.

High-harmonic generation can also occur due to the inhomogeneity of the pump pulse background, in an effect distinct from standard vacuum high-harmonic generation. For a probe pulse counterpropagating with a slowly varying background, this is predicted to occur at finite time during overlap of the probe and pump pulses at an order earlier (via four-photon scattering), than for those photons that reach a detector (via six-photon scattering)[79]. This finite-time signal disappears when the probe and pump pulses are well separated again, but is calculated to dominate the signal of frequency-shifted photons when the pulses overlap in this setup if $(E_s/E_{\rm cr})^2\omega_p\tau_s \ll 1$ for strong-pulse duration τ_s.

Gradient-dependent vacuum refractive index is a way to describe the addition to the standard predicted vacuum refractive index that occurs when the pump laser is time varying. This has been calculated for a probe propagating through the electric/magnetic antinode of a pump standing wave[36]. The change in vacuum refractive index $\Delta \mathsf{n}_{\rm vac}$ can be written in the form:

$$\Delta \mathsf{n}_{\rm vac}^{\parallel,\perp}(\varphi) = \frac{E_p}{E_p'}\mathsf{n}_{\rm vac}^{\parallel,\perp\prime}(\varphi). \tag{41}$$

In a setup of two colliding plane waves with no transverse structure, it was shown that this term is a surface term and is zero initially and finally, when the probe and background are well separated[79]. The contact term was also noted in a recent study of polarization flipping in arbitrary plane waves[37]. Although it has been suggested that this part of the interaction could be a useful probe of dark matter particles[36], a consistent finite-time calculation has yet to be performed to establish the nature of this effect.

4.6. Nonperfect vacua

In any realistic experiment, the vacuum will be synthetic and hence imperfect. Residue particles in interaction chambers will also be affected by intense laser pulses and can produce a source of background that may obscure the measurement of real photon–photon scattering. The Cotton–Mouton effect, in which a dilute gas becomes birefringent in the presence of an electromagnetic wave is just one such example[80]. In light of this, various proposals have been considered that instead use an altered vacuum to enhance the signal of vacuum polarization.

Resonant cavities can be employed in order to increase the sensitivity of whatever eigenfrequencies are resonant for that particular cavity[48]. For example, a cavity can be designed such that the frequency that is generated by vacuum four-wave mixing of two modes of the cavity, is resonant. This idea has been studied for the TE_{01} modes of such a cavity and the growth of the mixing signal in the form of the longitudinal standing-wave magnetic field, found to increase linearly with time[81] as

$$B_3(t) = \frac{itV}{2\omega_3} B_1^2 B_2^*,$$

https://doi.org/10.1017/hpl.2016.1 Published online by Cambridge University Press

for source magnetic standing-wave strengths B_1, B_2 and coupling constant V. The vacuum signal was predicted to be detectable if an electric field 2×10^{-8} times the critical Schwinger field was employed with a superconducting cavity with a resistance of 1 nΩ and a resonant, vacuum-mixing frequency of 13.2 μeV. This idea was refined[82] and the prediction made that 18 photons can be produced by a magnetic field of around 0.28 T in a cylindrical cavity of length 2.5 m, radius 25 cm and quality factor 4×10^{10}.

Real plasmas already have a refractive index different from unity, and this can combine with the shift of the refractive index due to vacuum polarization and lead to an enhancement. The system of equations by Akhiezer and Polovin[83] for the propagation of a circularly polarized plane wave through a cold collisionless plasma was updated to include the vacuum current in Maxwell's equations and also take into account collisions[84]. For the collisionless case, the modified refractive index of the combined system was found to be:

$$\mathsf{n} = \sqrt{\mathsf{n}_{\mathrm{pl}}^2 + \tfrac{1}{4}\delta\mathsf{n}_{\mathrm{vac}}^{\perp}(1-\mathsf{n}_{\mathrm{pl}}^2)^2}$$

with n_{pl} the plasma refractive index and $\delta\mathsf{n}_{\mathrm{vac}}^{\perp} = \mathsf{n}_{\mathrm{vac}}^{\perp} - 1$ as defined in Equation (26). Another detectable signal of photon–photon scattering has been calculated to exist when an overdense plasma channel is subjected to an intense laser beam[85]. In addition, the altered dispersion relation for electromagnetic waves due to vacuum polarization effects in a strongly magnetized cold plasma has been calculated[86–88], which is particularly relevant for the dynamics of strongly magnetized neutron stars.

5. Summary

There has been a proliferation of labels to describe polarization effects of the quantum vacuum due to intense laser pulses. However, as we have discussed, all of these are manifestations of the QED prediction that real photons can scatter off one another. The commonality of the main approaches of describing real photon–photon scattering, through calculation of the polarization operator, scattering matrix elements and Heisenberg–Euler-modified Maxwell equations, has been made manifest. Many signals of this long-predicted phenomenon, whether at the level of individual photons or at the level of electromagnetic fields, have been calculated and found measurable in experiments using high-intensity laser pulses. This implies that the first measurement of real photon–photon scattering will finally be performed in the near future.

References

1. C. Danson, D. Hillier, N. Hopps, and D. Neely, High Power Laser Sci. Eng. **3**, e3 (2015).
2. M. Marklund and P. K. Shukla, Rev. Mod. Phys. **78**, 591 (2006).
3. A. Di Piazza, C. Müller, K. Z. Hatsagortsyan, and C. H. Keitel, Rev. Mod. Phys. **84**, 1177 (2012).
4. D. Bernard, F. Moulin, F. Amiranoff, A. Braun, J. P. Chambaret, G. Darpentignz, G. Grillon, S. Ranc, and F. Perrone, Eur. Phys. J. D **10**, 141 (2000).
5. A. Cadène, P. Berceau, M. Fouché, R. Battesti, and C. Rizzo, Eur. Phys. J. D **68**, 16 (2014) arXiv:1302.5389.
6. F. Della Valle, E. Milotti, A. Ejlli, G. Messineo, L. Piemontese, G. Zavattini, U. Gastaldi, R. Pengo, and G. Ruoso, Phys. Rev. D **90**, 092003 (2014).
7. H. Schlenvoigt, T. Heinzl, U. Schramm, T. Cowan, and R. Sauerbrey, Phys. Scr. **91**, 023010 (2016).
8. S. Weinberg, *The Quantum Theory of Fields. Vol. 1: Foundations* (Cambridge University Press, 2005).
9. M. E. Peskin and D. V. Schroeder, *An Introduction to Quantum Field Theory* (Westview, 1995).
10. V. P. Gusynin and I. A. Shovkovy, J. Math. Phys. **40**, 5406 (1999).
11. G. V. Dunne and T. M. Hall, Phys. Rev. D **60**, 065002 (1999).
12. W. Heisenberg and H. Euler, Z. Phys. **98**, 714 (1936).
13. V. Weisskopf, Mat.-Fys. Medd. K. Dan. Vidensk. Selsk. **14**, 6 (1936).
14. J. Schwinger, Phys. Rev. **82**, 664 (1951).
15. F. Sauter, Z. Phys. **69**, 742 (1931).
16. B. De Tollis, Nuovo Cimento **35**, 1182 (1965).
17. A. Akhieser, L. Landau, and I. Pomeranchook, Nature **138**, 206 (1936).
18. A. Achieser, Phys. Z. Sov. **11**, 264 (1937).
19. V. B. Berestetskii, E. M. Lifshitz, and L. P. Pitaevskii, *Quantum Electrodynamics* 2nd edn (Butterworth-Heinemann, 1982).
20. J. S. Toll, "The dispersion relation for light and its application to problems involving electron pairs", PhD. Thesis (Princeton University Press, 1952).
21. N. B. Narozhnyĭ, Sov. Phys. JETP **28**, 371 (1969).
22. V. N. Baĭer, A. I. Mil'shteĭn, and V. M. Strakhovenko, Sov. Phys. JETP **42**, 961 (1976).
23. S. Meuren, C. H. Keitel, and A. Di Piazza, Phys. Rev. D **88**, 013007 (2013).
24. W. Dittrich and H. Gies, Springer Tracts Mod. Phys. **166**, 1 (2000).
25. A. Akhiezer and V. Berestetskii, *Quantum Electrodynamics* (Interscience, 1965).
26. A. Di Piazza, Ann. Phys. **338**, 302 (2013).
27. D. H. Delphenich, Nonlinear optical analogies in quantum electrodynamics, hep-ph/0610088.
28. N. B. Narozhny and A. M. Fedotov, Contemp. Phys. **56**, 249 (2015).
29. R. Baier and P. Breitenlohner, Acta Phys. Austriaca **25**, 212 (1967).
30. W. Dittrich and H. Gies, Phys. Rev. D **58**, 025004 (1998) hep-ph/9804375.
31. G. M. Shore, Nucl. Phys. B **778**, 219 (2007) hep-th/0701185.
32. S. Meuren, K. Z. Hatsagortsyan, C. H. Keitel, and A. Di Piazza, Phys. Rev. D **91**, 013009 (2015).
33. A. Ferrando, H. Michinel, M. Seco, and D. Tommasini, Phys. Rev. Lett. **99**, 150404 (2007).
34. P. Böhl, B. King, and H. Ruhl, Phys. Rev. A **92**, 032115 (2015).
35. B. King, P. Böhl, and H. Ruhl, Phys. Rev. D **90**, 065018 (2014).
36. H. Hu and J. Huang, Phys. Rev. A **90**, 062111 (2014).

https://doi.org/10.1017/hpl.2016.1 Published online by Cambridge University Press

37. V. Dinu, T. Heinzl, A. Ilderton, M. Marklund, and G. Torgrimsson, Phys. Rev. D **89**, 125003 (2014).
38. G. Boillat, J. Math. Phys. **11**, 941 (1970).
39. J. Plebanski, *Lectures on Nonlinear Electrodynamics*. Lectures on Nonlinear Electrodynamics, Nordita report RX-476.
40. I. Białynicki-Birula, in *Quantum Theory of Particles and Fields*, B. Jancewicz and J. Lukierski (eds) (World Scientific, 1983).
41. G. Torgrimsson, Ellipticity induced in vacuum birefringence, in *Theory and Experiment for Hadrons on the Light-Front (Light Cone 2014) Raleigh, North Carolina, USA, May 26–30, 2014*. arXiv:1409.8069.
42. V. Dinu, T. Heinzl, A. Ilderton, M. Marklund, and G. Torgrimsson, Phys. Rev. D **90**, 045025 (2014).
43. B. King and C. H. Keitel, New J. Phys. **14**, 103002 (2012).
44. A. Di Piazza, K. Z. Hatsagortsyan, and C. H. Keitel, Phys. Rev. Lett. **97**, 083603 (2006).
45. B. King, A. Di Piazza, and C. H. Keitel, Phys. Rev. A **82**, 032114 (2010).
46. T. Heinzl, B. Liesfeld, K.-U. Amthor, H. Schwoerer, R. Sauerbrey, and A. Wipf, Opt. Commun. **267**, 318 (2006).
47. B. King, "Vacuum polarisation effects in intense laser fields", PhD. Thesis (University of Heidelberg, 2010).
48. J. D. Jackson, *Classical Electrodynamics* (John Wiley & Sons, 1975).
49. L. Levi, *Applied Optics* (John Wiley & Sons, 1968).
50. B. King, A. D. Piazza, and C. H. Keitel, Nature Photon. **4**, 92 (2010).
51. D. Tommasini and H. Michinel, Phys. Rev. A (R) **82**, 011803 (2010).
52. G. Y. Kryuchkyan and K. Z. Hatsagortsyan, Phys. Rev. Lett. **107**, 053604 (2011).
53. Y. Monden and R. Kodama, Phys. Rev. Lett. **107**, 073602 (2011).
54. A. Paredes, D. Novoa, and D. Tommasini, Phys. Rev. A **90**, 063803 (2014).
55. F. Karbstein, H. Gies, M. Reuter, and M. Zepf, Phys. Rev. D **92**, 071301 (2015) arXiv:1507.0108.
56. H. Gies, F. Karbstein, and N. Seegert, New J. Phys. **15**, 083002 (2013).
57. H. Gies, F. Karbstein, and N. Seegert, New J. Phys. **17**, 043060 (2015).
58. J. V. Moloney and A. C. Newell, *Nonlinear Optics* (Westview Press, 2004).
59. E. Lundström, G. Brodin, J. Lundin, M. Marklund, R. Bingham, J. Collier, J. T. Mendonça, and P. Norreys, Phys. Rev. Lett. **96**, 083602 (2006).
60. F. Fillion-Gourdeau, C. Lefebvre, and S. MacLean, Phys. Rev. A **91**, 031801 (2015).
61. A. Di Piazza, K. Z. Hatsagortsyan, and C. H. Keitel, Phys. Rev. D **72**, 085005 (2005).
62. A. M. Fedotov and N. B. Narozhny, Phys. Lett. A **362**, 1 (2007).
63. M. Lutzky and J. S. Toll, Phys. Rep. **113**, 1649 (1959).
64. Z. Bialynicka-Birula, Physica D **2**, 513 (1981).
65. V. V. Zheleznyakov and A. L. Fabrikant, Sov. Phys. JETP **55**, 794 (1982).
66. N. N. Rozanov, Sov. Phys. JETP **76**, 991 (1993).
67. J. S. Heyl and L. Hernquist, Phys. Rev. D **58**, 043005 (1998).
68. J. S. Heyl and L. Hernquist, Phys. Rev. D **59**, 045005 (1999).
69. A. Di Piazza, A. I. Milstein, and C. H. Keitel, Phys. Rev. A **76**, 032103 (2007).
70. D. Tommasini, A. Ferrando, H. Michinel, and M. Seco, Phys. Rev. A **77**, 042101 (2008).
71. D. Tommasini, A. Ferrando, M. Humberto, and M. Seco, J. High Energy Phys. **11**, 43 (2009).
72. K. Homma, D. Habs, and T. Tajima, Appl. Phys. B **104**, 769 (2011).
73. A. M. Fedotov, Proc. SPIE **6726**, 67261D (2007).
74. D. Kharzeev and K. Tuchin, Phys. Rev. A **75**, 043807 (2007).
75. M. Marklund, G. Brodin, and L. Stenflo, Phys. Rev. Lett. **91**, 163601 (2003).
76. M. Marklund, B. Eliasson, and P. K. Shukla, Sov. Phys. JETP **79**, 208 (2004).
77. S. C. Wilks, J. M. Dawson, W. B. Mori, T. Katsouleas, and M. E. Jones, Phys. Rev. Lett. **62**, 2600 (1989).
78. J. T. Mendonca, M. Marklund, P. K. Shukla, and G. Brodin, Phys. Lett. A **359**, 700 (2006).
79. B. King, P. Böhl, and H. Ruhl, Phys. Rev. D **90**, 065018 (2014).
80. G. Zavattini, U. Gastaldi, R. Pengo, G. Ruoso, F. Della Valle, and E. Milotti, Int. J. Mod. Phys. A **27**, 1260017 (2012).
81. G. Brodin, M. Marklund, and L. Stenflo, Phys. Rev. Lett. **87**, 171801 (2001).
82. D. Eriksson, G. Brodin, M. Marklund, and L. Stenflo, Phys. Rev. A **70**, 013808 (2004).
83. A. I. Akhiezer and R. V. Polovin, J. Exp. Theor. Phys. **3**, 696 (1956).
84. A. Di Piazza, K. Z. Hatsagortsyan, and C. H. Keitel, Phys. Plasmas **14**, 032102 (2007).
85. B. Shen, M. Y. Yu, and X. Wang, Phys. Plasmas **10**, 4570 (2003).
86. G. Brodin, M. Marklund, L. Stenflo, and P. K. Shukla, New J. Phys. **8**, 16 (2006).
87. J. Lundin, L. Stenflo, G. Brodin, M. Marklund, and P. K. Shukla, Phys. Plasmas **14**, 6 (2007).
88. P. K. Shukla and L. Stenflo, J. Plasma Phys. **74**, 719 (2008).

https://doi.org/10.1017/hpl.2016.1 Published online by Cambridge University Press